THREE-DIMENSIONAL LINEAR FRACTURE MECHANICS ANALYSIS BY A DISPLACEMENT-HYBRID FINITE-ELEMENT MODEL

S.N. ATLURI, K. KATHIRESAN

School of Engineering Science and Mechanics, Georgia Institute of Technology, Atlanta, Georgia 30332, U.S.A.

A.S. KOBAYASHI

Department of Mechanical Engineering, University of Washington, Seattle, Washington 98105, U.S.A.

SUMMARY

This paper deals with a finite-element procedure for the calculation of modes I, II and III stress intensity factors, which vary, along an arbitrarily curved three-dimensional crack front in a structural component. The finite-element model is based on a modified variational principle of potential energy with relaxed continuity requirements for displacements at the interelement boundary. The variational principle is a three-field principle, with the arbitrary interior displacements for the element, interelement boundary displacements, and element boundary tractions as variables. The unknowns in the final algebraic system of equations, in the present displacement-hybrid finite element model, are the nodal displacements and the three elastic stress intensity factors. Special elements, which contain proper square root and inverse square root crack front variations in displacements and stresses, respectively, are used in a fixed region near the crack front. Interelement displacement compatibility is satisfied, by assuming an independent interelement boundary displacement field, and using a Lagrange multiplier technique to enforce such interelement compatibility. These Lagrangean multipliers, which are physically the boundary tractions, are assumed from an equilibrated stress field derived from three-dimensional Beltrami (or Maxwell-Morera) stress functions that are complete. However, considerable care should be exercised in the use of these stress functions such that the stresses produced by any of these stress function components are not linearly dependent.

Since the method is based on a rigorous variational principle, which enforces at least on an average the condition of interelement displacement continuity when $\sqrt{r}$ type displacements are included in the near-tip region, the convergence of the finite element solution for nodal displacements as well as the stress intensity factors is established mathematically. The geometry of the "basic element" used presently, is a 20 node isoparametric brick element, with 60 degrees of freedom per element. The relevant matrices are evaluated numerically, using non-product type quadrature formulae with proper mathematical transformations being used when singular type functions are encountered in stresses and strains in the near-tip region.

The utility of the formulation is demonstrated through numerical results for the problem of a through-the-thickness crack in a finite width plate subjected to combined tension, in-plane shear and out-of-plane shear. In analyzing this problem the controversy regarding the singularity where the crack tip intersects the flat surface has been recognized and attempts have been made to assess the three-dimensional influence of the flat surface on the two-dimensional intensity factors. The second problem that is currently being investigated is that of a slanted, semi-elliptical surface flaw in a tension plate. The preliminary results from the present three-dimensional formulation, and extensive results for the two-dimensional problems based on similar formulations and published earlier, lead us to believe that the present method is a fast and economical (requiring fewer elements compared to majority of other methods, and leading to a direct calculation of intensity factors) method for studying the linear fracture mechanics of cracked structural components.

Introduction: During the past decade fracture mechanics has been successfully used to analyze failed structural components, certifying a structure for its intended use, and correlating cyclic or sustained stress growth of flaws. In applying fracture mechanics to practical problems, the analyst must know the stress intensity factors of the flaw as well as material characteristics such as the fracture toughness, cyclic crack growth rates, and sustained stress crack growth rate in order to assess the situation. Unfortunately, available solutions of stress intensity factors are limited to idealized flaws of simple geometries and loading conditions and thus considerable engineering judgement is required before they can be used to estimate stress intensity factors of complex flaws which exist in actual problems.

Among the limited analytical solutions to three-dimensional "mode I" crack problems can be mentioned the solutions of Sneddon [1] for the penny-shaped crack, Sternberg and Sadowsky [2] for an ellipsiodal cavity under uniform remote tension, Green and Sneddon [3] for an elliptical crack under uniform remote tension, Shah and Kobayashi [4,5] for semi-elliptical surface flaws, and Smith et.al. [6,7] for segment-of-a-circle surface flaw. Available solutions for mixed mode three-dimensional problems, on the other hand, are limited to that of an embedded elliptical flaw in an infinite solid, Kassir and Sih [8]. Thus the prediction of stress-intensity factors in three-dimensional problems, involving irregularly shaped surface flaws and embedded flaws in arbitrary shaped structural problems, and under arbitrary (modes I, II and III) loading necessitates the use of a numerical method such as the finite element method.

One of the requisites of solving any crack problem by numerical method is to handle the stress singularities at the crack tips properly. This involves a knowledge of the correct behavior of singularities, a task accomplished by analytical means in finding the asymptotic solution in the vicinity of the crack front. It is essential, for the convergence of the numerical method such as the finite element method (Tong and Pian [9]), to preserve this singular behavior of the solution in the problem by embedding such singular functions in assumed stress and strain fields in finite elements in the vicinity of the crack. Such "embedded-singularity" elements have been extensively developed in the recent years for two dimensional problems. Among these can be mentioned the works of Byskov [10] whose finite element formulation violates the inter-element displacement compatibility criteria, Pian, Tong and Luk [11, see also 12] who use a hybrid-stress finite element model, and Atluri, Kobayashi and Nakagaki [13,14] who use a hybrid-displacement model in satisfying the inter-element displacement and traction continuity. These "hybrid" models offer the advantage that the stress intensity factors can be calculated directly, as unknowns in the finite element equations for the structure, and that the convergence of the finite element solutions for the displacements in the structure as well as the stress-intensity factors can be established mathematically.

In the following we present the formulation and evaluation of an "embedded-singularity" element based on the assumed displacement hybrid model for the calculation of stress-intensity factors which vary along an arbitrary shaped crack front in a three-dimensional structural component.

2. Theoretical Considerations of Cracks in Three-Dimension: In the macroscopic (continuum) theories of fracture mechanics there are generally three types of problems which are: (a) the solution of the mechanics problem for the given geometry and applied loads to determine

the "stress-intensity factors" representing the severity of applied loads and corresponding to the conjectured modes of fracture such as brittle, ductile or quasi-ductile fracture, (b) experimental work to determine the resistance of material to fracture, quantified by parameters such as the "characteristic strength parameters" and (c) development of an appropriate fracture criterion, which is nothing but the direct comparison of "characteristic strength parameters" to calculated "stress-intensity factors" or a function of these stress-intensity factors. Consider an arbitrary shaped flaw in an arbitrarily loaded three-dimensional structural component, as shown in Fig. 1. The stress intensity factors K_1, K_2 and K_3 which may occur simultaneously in three-dimensional problems under arbitrary loading conditions, are defined as,

$$K_1(t) = \lim_{r\to 0} \sqrt{2r}\,\sigma_{zz}(\theta=0);\; K_2(t) = \lim_{r\to 0} \sqrt{2r}\,\sigma_{nz}(\theta=0);\; K_3 = \lim_{r\to 0} \sqrt{2r}\,\sigma_{tz}(\theta=0) \tag{1}$$

Thus K_1, K_2 and K_3 may also vary from point to point along the crack border, defined by coordinate t. In terms of these factors, the asymptotic solution for displacements and stresses in the immediate neighborhood of a crack front have been shown [8] to be,

$$u_n = \frac{K_1(2r)^{\frac{1}{2}}}{2\mu} \cos\frac{\theta}{2}\left[(1-2\nu) + \sin^2\frac{\theta}{2}\right] + \frac{K_2(2r)^{\frac{1}{2}}}{2\mu}\left[2(1-\nu) + \cos^2\frac{\theta}{2}\right] + O(r) \tag{2a}$$

$$u_t = \frac{K_3(2r)^{\frac{1}{2}}}{\mu} \sin\frac{\theta}{2} + O(r) \tag{2b}$$

$$u_z = \frac{K_1(2r)^{\frac{1}{2}}}{2\mu} \sin\frac{\theta}{2}\left[2(1-\nu) - \cos^2\frac{\theta}{2}\right] - \frac{K_2(2r)^{\frac{1}{2}}}{2\mu}\cos\frac{\theta}{2}\left[(1-2\nu) - \sin^2\frac{\theta}{2}\right] + O(r) \tag{2c}$$

$$\sigma_n = \frac{K_1}{4(2r)^{\frac{1}{2}}}\left(3\cos\frac{\theta}{2} + \cos\frac{5\theta}{2}\right) - \frac{K_2}{4(2r)^{\frac{1}{2}}}\left(7\sin\frac{\theta}{2} + \sin\frac{5\theta}{2}\right) + O(r) \tag{3a}$$

$$\sigma_t = \frac{K_1}{(2r)^{\frac{1}{2}}} 2\nu\cos\frac{\theta}{2} - \frac{K_2}{(2r)^{\frac{1}{2}}} 2\nu\sin\frac{\theta}{2} + O(r) \tag{3b}$$

$$\sigma_z = \frac{K_1}{4(2r)^{\frac{1}{2}}}\left(5\cos\frac{\theta}{2} - \cos\frac{5\theta}{2}\right) - \frac{K_2}{4(2r)^{\frac{1}{2}}}\left(\sin\frac{\theta}{2} - \sin\frac{5\theta}{2}\right) + O(r) \tag{3c}$$

$$\sigma_{tz} = \frac{K_3}{(2r)^{\frac{1}{2}}}\cos\frac{\theta}{2} + O(r) \tag{3d}$$

$$\sigma_{zn} = -\frac{K_1}{4(2r)^{\frac{1}{2}}}\left(\sin\frac{\theta}{2} - \sin\frac{5\theta}{2}\right) + \frac{K_2}{4(2r)^{\frac{1}{2}}}\left(3\cos\frac{\theta}{2} + \cos\frac{5\theta}{2}\right) + O(r) \tag{3e}$$

$$\sigma_{nt} = -\frac{K_3}{(2r)^{\frac{1}{2}}}\sin\frac{\theta}{2} + O(r) \tag{3f}$$

where μ is the shear modulus, and ν is the Poisson ratio. It can be shown [15] that using Eqs. (2 and 3), the strain energy density (per unit volume, $W \equiv S(\theta)/r$) near the crack front may be written as,

$$\frac{(16\mu)S(\theta)}{r} = \left(a_{11}K_1^2 + 2a_{12}K_1K_2 + a_{22}K_2^2 + a_{33}K_3^2\right)/r \tag{4}$$

where, $a_{11} = [(3-4\nu-\cos\theta)(1+\cos\theta)]$; $a_{12} = 2\sin\theta\,[\cos\theta-(1-2\nu)]$; $a_{22} = [4(1-\nu)(1-\cos\theta) + (1+\cos\theta)(3\cos\theta-1)]$; and $a_{33} = 4$.

It can be stated that the formulation of fracture criterion for general, mixed-mode, three-dimensional problems is still an open subject. Sih [15] has proposed such a fracture criterion based on the strain-energy-density concept, and may be stated as: (1) the crack grows in a direction, $\theta = \theta_c$, for which $S(\theta)$ reaches a relative minimum, (2) the crack growth begins when the value of $S\ (K_1,K_2,K_3)$ at $\theta = \theta_c$ reaches a critical value S_c, which is a material parameter.

Based on the fact that an appropriate fracture-criterion may be formulated and implemented when once the intensity factors $K_1(t)$, $K_2(t)$ and $K_3(t)$ are known, the primary objective of this paper and computational fracture mechanics in general, is to accurately calculate the stress intensity factors for arbitrary shaped flaws under general loading conditions.

3.1 <u>The Hybrid-Displacement Finite Element Model</u>: In as much as the most commonly used compatible displacement finite element model with polynomial basis functions in each element cannot represent the asymptotic singular stress and strain fields in the vicinity of the crack boundary, an alternate finite element formulation is needed. In such a formulation, one should be able to incorporate the exact asymptotic form of solution for singular stresses and strains in elements in a fixed region near the crack boundary (near-field), and use only regular polynomial type basis functions in elements in the far field. Inter-element continuity of displacements and traction must also be maintained between the near-field elements (with singular basis functions) and the far field elements (with regular polynomial basis functions). One such formulation is the assumed displacement hybrid finite element model which has been previously used in two-dimensional problems of fracture mechanics [13, 14], and is extended in this paper to a three-dimensional formulation. We consider the solid to be descritized into a union of finite number of finite-sized three-dimensional elements which have piecewise continuous boundaries at which neighboring elements join. We denote the sub-domain of each finite element by Ω_m and its boundary by $\partial\Omega_m$. We denote that portion of $\partial\Omega_m$ which is common to an adjacent element by ρ_m (inter-element boundary), that portion where tractions are prescribed by S_{σ_m}, and that portion where displacements are prescribed by S_{u_m}. Thus, $\partial\Omega_m = \rho_m + S_{\sigma_m} + S_{u_m}$. It may happen that, for certain elements which do not adjoin the overall boundary of Ω, $S_{\sigma_\ell} = S_{u_\ell} = 0$ and hence, $\partial\Omega_\ell = \rho_\ell$. While traversing along ρ_m, we arbitrarily denote the left hand side vicinity (in the limit as ρ_m is approached) by superscript (+) and the right hand side by a (-). It is also worth noting that in an integral such as $\sum_m \int_{\rho_m} F(\rho)\, d\rho$ to be considered below, each segment of the element boundary occurs twice because it is on the boundary of two adjacent domains, say Ω_m and Ω_{m+1}.

With this notation suppose $\Omega_m(m = 1,\ldots n)$ be the elements immediately adjacent to the crack boundary as in Fig. 1 (i.e., in the near field), and $\Omega_m(m = n{+}1\ldots M)$ be the elements in the far field. Thus singular type strains and stresses will be assumed in the elements $\Omega_m(m = 1,\ldots n)$ and regular type strains will be assumed in elements $\Omega_m(m = n{+}1,\ldots M)$. In constructing the general finite element model, based on assumed displacements, let u_i in each Ω_m $(m = 1\ldots N)$ be arbitrary (and this can include $\sqrt{r}$ type functions in Ω_m, $m = 1,\ldots n)$ such that $u_i^+ \neq u_i^-$ and $T_i^+ \neq T_i^-$, a priori, at ρ_m. Let $\epsilon_{ij} = \frac{1}{2}(u_{i,j} + u_{j,i})$ and $\sigma_{ij} = E_{ijK\ell}\epsilon_{K\ell}$ in each Ω_m. With these a priori conditions, it can be shown [13,14] that the three-field variational principle governing the hybrid-displacement model is based on the modified potential energy functional,

$$\pi(u_i, T_{i\rho}, \tilde{u}_{i\rho}) = \sum_{m=1}^{M} \left\{ \int_{\Omega_m} \left[\frac{1}{2} E_{ijk\ell} \epsilon_{ij} \epsilon_{k\ell} - \bar{F}_i u_i \right] d\Omega - \int_{S_{\sigma_m}} \bar{T}_i u_i dS \right.$$

$$+ \int_{S_{u_m}} T_i (u_i - \bar{u}_i) - \int_{\rho_m} T_{i\rho} (u_i - \tilde{u}_{i\rho}) \, d\rho . \tag{5}$$

where: (1) u_i are assumed displacements inside Ω_m, (2) $\tilde{u}_{i\rho}$ are independently assumed displacements on ρ_m, and are common to elements adjoining at ρ_m, and (3) $T_{i\rho}$ are Lagrange multipliers, assumed independently for each element on its boundary. The equation $\delta\pi = 0$ with respect to variations in u_i, $T_{i\rho}$ and $\tilde{u}_{i\rho}$ can be shown to lead to the Euler equations: (a) equilibrium equation, $\sigma_{ij,j} + \bar{F}_i = 0$ in Ω_m, (b) traction condition $\sigma_{ij} m_j \equiv T_i = \bar{T}_i$ on S_{σ_m}, (c) inter-element displacement continuity condition $u_i^+ = u_i^- = \tilde{u}_{i\rho}$ at ρ_m; (d) inter-element traction equilibrium condition $T_i^+ = T_{i\rho}^+ = T_{i\rho}^- = T_i^-$ on ρ_m and (e) the displacement condition $u_i = \bar{u}_i$ on S_{u_m}. The discrete approximations for each of the above field variables can be assumed as follows:

(i) Near-field Elements: Ω_m ($m = 1,\ldots n$).

$$\{u_i\} = [U_R]\{\beta\} + [U_S]\begin{Bmatrix} K_1 \\ K_2 \\ K_3 \end{Bmatrix} \; ; \; \{\tilde{u}_{i\rho}\} = [L_S]\{q\} \; ; \; \{T_{i\rho}\} = [R_S]\{\alpha\} \tag{6}$$

(ii) Far-field Elements: Ω_m ($m = n+1\ldots N$).

$$\{u_i\} = [U_R]\{\beta\} \; ; \; \{\tilde{u}_{i\rho}\} = [L]\{q\} \; ; \; \{T_{i\rho}\} = [R]\{\alpha\} \tag{7}$$

In the above $[U_R]$ are arbitrary polynomial functions, $[U_S]$ are asymptotically correct near field solution functions as given by Eq. (2); $[L_S]$ are interpolates for boundary displacements of near-field elements interms of element generalized displacement coordinates q at nodes on the boundary, R_S are arbitrary basis functions for boundary tractions on the near-field element, and similar interpretations are given for $[U_R]$, $[L]$ and $[R]$ pertinent to the far field element.

It can be shown [16] that for the successful implementation of this finite element model the number of β's in Eqs. (6,7) should, in general, be greater than or at least equal to the number of α's, plus the number of rigid body modes for each element. It is also shown [14,15] that considerable numerical simplification would arise if number of β's is equal to the number of α's plus the number of rigid body modes for each element, and this condition is satisfied in the present formulation. By using the Eqs. (6,7) in Eq. (5), eliminating α's and β's for each element in terms of element nodal displacements and noting the connectivity of nodal displacements of neighboring elements, the functional in Eq. (5) can be expressed as a function of independent global generalized displacements q* and the stress intensity factor vector $\underset{\sim}{K}$ [13]. The variation of $\pi(\underset{\sim}{q}^*, \underset{\sim}{K})$ leads to the final element equations, as shown in Ref. [13]; of the form,

$$\left[\begin{array}{c|c} K_1 & K_2^T \\ \hline K_2 & K_3 \end{array}\right] \begin{Bmatrix} \underset{\sim}{q}^* \\ \hline \underset{\sim}{K} \end{Bmatrix} = \begin{Bmatrix} \underset{\sim}{Q}_1 \\ \hline \underset{\sim}{Q}_2 \end{Bmatrix} \tag{8, 9}$$

From which $\underset{\sim}{q}^*$ and the stress-intensity factors $\underset{\sim}{K}$ are directly solved for.

3.2 Geometry of the Finite Elements: The geometrical shape of the element in cartesian coordinates is a general "brick" element with six quadratically curved surfaces and with twenty nodes, as shown in Fig. 2. If x, y, z are cartesian coordinates, we introduce curvilinear coordinates ξ, η, ζ $(-1 < \xi,\eta,\zeta < +1)$, such that the relation between the two coordinates is given by

$$X = \sum_{i=1}^{20} N_i(\xi,\eta,\zeta)\, x_i \;;\; y = \sum_{i=1}^{20} N_i(\xi,\eta,\zeta)\, y_i \;;\; z = \sum_{i=1}^{20} N_i(\xi,\eta,\zeta)\, z_i \tag{10}$$

where (x_i, y_i, z_i) are the cartesian coordinates of the i^{th} node $(i = 1,20)$ of the element.

The form of the functions N_i can readily be obtained from the well-known "isoparametric" element theory of Zienkiewicz et al. The Jacobian of the coordinate transformation implied in Eq. (10) is defined as,

$$[J] = \left[\frac{\partial(x,y,z)}{\partial(\xi,\eta,\zeta)}\right] \tag{11}$$

With the displacements u (x direction), v (y direction) and w (in z direction) as degrees of freedom at each node, the present element has 60 kinematic degrees of freedom.

In the subsequent sections, the assumptions for u_i, $T_{i\rho}$ and $\tilde{u}_{i\rho}$ mentioned in Section 3.1, are given only for the so-called "singular" elements near the crack boundary, for want of space. The construction of these signular elements with embedded singularities, is the crux of the problem; however, by omitting all the singular functions in the field variables and choosing appropriate regular functions to replace them, the "regular" elements for use in the far field can easily be constructed [13].

3.3 Element-Interior Displacement Field (Singular Element):

For a near field ("singular") element, the $[U_R]\{\beta\}$ part of the element displacement field $\{u_i\}$ as in Eq. (6) is assumed as,

$$\begin{aligned} u_R = {} & \beta_1\xi + \beta_2\eta + \beta_3\xi + \beta_4\xi\eta + \beta_5\eta\zeta + \beta_6\zeta\xi + \beta_7\xi^2 + \beta_8\eta^2 + \beta_9\zeta^2 + \beta_{10}\xi^3 \\ & + \beta_{11}\xi\eta^2 + \beta_{12}\xi\zeta^2 + \beta_{13}\xi^2\eta + \beta_{14}\eta^3 + \beta_{15}\xi^4 + \beta_{16}\xi^2\zeta + \beta_{17}\xi^2\zeta^2 + \beta_{18}\xi^3 \\ & + \beta_{19}\xi\eta\zeta + \text{rigid body modes} \end{aligned}$$

$$\begin{aligned} v_R = {} & \beta_2\xi + \beta_{20}\eta + \beta_{21}\zeta + \beta_{22}\xi\eta + \beta_{23}\eta\zeta + \beta_{24}\zeta\xi + \beta_{25}\xi^2 + \beta_{26}\eta^2 + \beta_{27}\zeta^2 \\ & + \beta_{28}\xi^3 + \beta_{29}\xi\eta^2 + \beta_{30}\eta^4 + \beta_{31}\xi^2\eta + \beta_{32}\eta^3 + \beta_{33}\eta\zeta^2 + \beta_{34}\eta^2\zeta^2 + \beta_{35}\eta^2\zeta \\ & + \beta_{36}\zeta^3 + \beta_{37}\xi\eta\zeta + \text{rigid body modes.} \end{aligned}$$

$$\begin{aligned} w_R = {} & \beta_3\xi + \beta_{21}\eta + \beta_{38}\zeta + \beta_{39}\xi\eta + \beta_{40}\eta\zeta + \beta_{41}\zeta\xi + \beta_{42}\xi^2 + \beta_{43}\eta^2 + \beta_{44}\zeta^2 \\ & + \beta_{45}\xi^3 + \beta_{46}\xi\eta^2 + \beta_{47}\zeta^4 + \beta_{48}\eta^2\zeta^2 + \beta_{49}\eta^3 + \beta_{50}\eta\zeta^2 + \beta_{51}\xi^2\zeta + \beta_{52}\eta^2\zeta \\ & + \beta_{53}\zeta^3 + \beta_{54}\xi\eta\zeta + \text{rigid body modes.} \end{aligned} \tag{12}$$

Thus a total of 60 polynomial basis functions are assumed for the displacements, out of which 54 produce strains and the other 6 are rigid body modes. Care has been excercised to see that even in limiting cases, any of the 54 "straining modes" do not degenerate to rigid-body modes. For the "singular" element the asymptotically correct solution as given in Eqs. (2) is assumed in addition, as shown in Eq. (6), with the stress-intensity factors being used directly as undetermined parameters. By properly evaluating the cartesian derivatives of the displacements given in Eqs. (12), the element strains are evaluated. Upon substitution for the total displacements, the element strain energy can be written as,

$$\int_{\Omega_m} \frac{1}{2} E_{ijk\ell}\epsilon_{ij}\epsilon_{k\ell} \equiv \frac{1}{2}\int_{\Omega_m} \left[E_{ijk\ell}\epsilon^R_{ij}\epsilon^R_{k\ell} + E_{ijk\ell}\epsilon^S_{ij}\epsilon^S_{k\ell} + 2E_{ijk\ell}\epsilon^R_{ij}\epsilon^S_{k\ell}\right] d\Omega \tag{13}$$

where the superscripts R and S refer to "regular" and "singular" respectively. It can be seen that the second integrand above has a $1/r$ singularity, where as the third integrand has a $1/\sqrt{r}$ singularity. However, since the asymptotic displacement field u^S_i in Eq. (2) corresponds to an equilibrium solution, one can, upon application of the divergence theorem write,

$$\int_{\Omega_m} E_{ijk\ell}\epsilon^S_{ij}\epsilon^S_{ij}\, d\Omega = \int_{\partial\Omega_m} T^S_i u^S_i\, dS \quad (14a) \qquad \int_{\Omega_m} E_{ijk\ell}\epsilon^S_{ij}\epsilon^R_{k\ell}\, d\Omega = \int_{\partial\Omega_m} T^S_i u^R_i\, ds \quad (14b)$$

Thus, since T^S_i has a $1/\sqrt{r}$ variation and u^S_i has a $\sqrt{r}$ variation, it can be seen that the r.h.s. integrand in Eq. (14a) is free of singularities, where as r.h.s integrand in Eq. (14b) has a "milder" $1/\sqrt{r}$ type singularity. This facilitates accurate numerical computations.

3.4 Element Boundary Displacements (Singular Element):

As discussed in Section 3.1, the boundary displacement $\tilde{u}_{i\rho}$ should be common at ρ_m for neighboring elements. This is accomplished by interpolating for $\tilde{u}_{i\rho}$ on a segment of ρ_m in terms of the nodal displacement coordinates on the particular segment of ρ_m only. Thus, considering the singular element such as ABCDEFGH in Fig. (2b), the following boundary displacements are assumed.

3.4.1. Face ABEF (ζ = -1):

$$u = a_o + a_1\sqrt{r} + a_2\eta + a_3 r + a_4\eta^2 + a_5\sqrt{r}\,\eta + a_6 r\eta + a_7\sqrt{r}\,\eta^2 \tag{15}$$

where r is the radius (dimensional) measured normal to the crack boundary. It can thus be seen that the displacements on Face ABEF (plane of the crack) has the asymptotically correct $\sqrt{r}$ variation. The parameters $(a_0, a_1, \ldots a_7)$ are determined uniquely in terms of the relevant u-displacement coordinates on ABEF, viz., q_1, q_2, q_3, q_4, q_{10}, q_{13}, q_{14}, q_{15} (see Fig. 2b). Thus this boundary displacement would be the same for two singular elements joining at face ABEF. Similar interpolates are used for the other two displacements, v and w.

3.4.2. Face CDHG (ζ = + 1):

Since this face is remote from the crack boundary, the displacements on this segment of the boundary can be regular polynomials. Thus, for instance, the u displacement on this face is interpolated uniquely in terms of the relevant model displacements q_5, q_6, q_7, q_{11}, q_{12}, q_{17}, q_{18}, q_{19}, as:

$$u = q_5\,(1+\xi)(1-\eta)(\xi-\eta-1)/4 + q_6\,(1-\xi^2)(1-\eta)/2 + q_7\,(1-\xi) \times (1-\eta)(-\xi-\eta-1)/4$$

$$+\, q_{11}\,(1+\xi)(1-\eta^2)/2 + q_{12}\,(1-\xi)(1-\eta^2)/2 + q_{17}\,(1+\xi)(1+\eta)(\xi+\eta-1)/4$$

$$+ q_{18}\ (1-\xi^2)(1+\eta)/2 + q_{19}\ (1-\zeta)(1+\eta) \times (-\xi+\eta+1)/4. \tag{16}$$

Identical interpolates are used for v and w in terms of thin respective nodal generalized coordinates. Equation (16) represents a unique quadratic interpolation for displacements u,v,w on face CDHG and hence is automatically compatible with the boundary displacements of regular (far-field element) that adjoins the present singular element at surface CDHG.

3.4.3. Faces ABCD and EFGH (η = - 1 and + 1):

On these faces, which are perpendicular to the crack front, the asymptotic solution for displacements indicates not only a $\sqrt{r}$ variation, but a rapid variation with θ. To reflect this, for instance, the displacements on face ABCD are assumed as,

$$u = a_o + a_1\xi + a_2\zeta + a_3 r + a_4\sqrt{r}\ \sin\frac{\theta}{2}\left(2 - 2\nu - \cos^2\frac{\theta}{2}\right)$$

$$+ a_5\sqrt{r}\ \cos\frac{\theta}{2}\left(1 - 2\nu - \sin^2\frac{\theta}{2}\right) + a_6\sqrt{r}\ \cos\frac{\theta}{2}\left(1 - 2\nu + \sin^2\frac{\theta}{2}\right)$$

$$+ a_7\sqrt{r}\ \sin\frac{\theta}{2}\left(2 - 2\nu + \cos^2\frac{\theta}{2}\right)\ . \tag{17}$$

and identical displacements v and w, with $(a_0 \ldots a_7)$ above, being replaced by $(b_0 \ldots b_7)$ and $(c_0 \ldots C_7)$ respectively. The parameters $(a_0 \ldots a_7)$ are uniquely found from (q_1 thru q_8); $(b_0 \ldots b_7)$ are found from (q_{41} thru q_{47}); and $(c_0 \ldots C_7)$ are found from (q_{21} thru q_{27}). An interpolate similar to that in Eq. (17) is likewise used for each of the three displacements is likewise on face EFGH. It is clear that when other "singular" elements adjoin the present element at faces ABCD and EFGH, the inter-element displacements are compatible.

3.4.4. Face ADHE (ξ = -1):

Similar to the interpolate on face ABEF, we assume,

$$u = a_0 + a_1\sqrt{r} + a_2\eta + a_3 r + a_4\eta^2 + a_5\sqrt{r}\ \eta + a_6 r\eta + a_7\sqrt{r}\ \eta^2 \tag{18}$$

where the constants $(a_0 \ldots a_7)$ are evaluated in terms of (q_1, q_7, q_8, q_9, q_{12}, q_{13}, q_{19} and q_{20}). Similar interpolates for v and w are assumed.

3.4.5. Face BCGH (ξ = + 1):

Similar to that on face CDHG, the interpolate for u is,

$$u = q_3(1-\eta)(1-\zeta)(-\eta-\zeta-1)/4 + q_4\ (1-\zeta^2)(1-\eta)/2 + q_5\ (1-\eta)(1+\zeta)(-\eta+\zeta-1)/4$$

$$+ q_{10}\ (1-\eta^2)(1-\zeta)/2 + q_{11}\ (1-\eta^2)(1+\zeta)/2 + q_{15}\ (1+\eta)(1-\zeta)(\eta-\zeta-1)/4$$

$$+ q_{16}\ (1-\zeta^2)(1+\eta)/2 + q_{17}\ (1+\eta)(1+\zeta)(\eta+\zeta-1)/4. \tag{19}$$

3.5 Element Boundary Tractions (Singular Element):

In this regard, we first note one of the relevant Euler equations of the present variational principle, which states that the boundary tractions generated by the assumed element-interior displacements u_i must match the independently assumed boundary tractions $T_{i\rho}$ at ρ_m and further that $(T_{i\rho})^+ = T_{i\rho}^-$. This can be stated precisely as,

$$\frac{1}{2}\left[E_{ijk\ell}\ (u_{k,\ell} + u_{\ell,k})\ \nu_j\right]^+ = T_{i\rho}^+ = T_{i\rho}^- = \left[E_{ijk\ell}\ (u_{k,\ell} + u_{\ell,k})\ \nu_j\right]^-/2 \tag{20}$$

Thus, since the assumed u_i include a $\sqrt{r}$ variation for the singular element, the boundary tractions generated by these u_i would have a $1/\sqrt{r}$ variation. Thus it can be seen that for numerical accuracy, the assumed tractions $T_{i\rho}$ for the singular element must also contain a $1/\sqrt{r}$ behavior (from a purely mathematical point of view when $T_{i\rho}$ are Lagrange multipliers, this condition is not immediately apparent). Since the displacement field u_i, in addition to satisfying Eq. (20), is also forced to satisfy the equilibrium equations through the variational principle, it can be seen that better accuracy in the formulation is achieved if the assumed $T_{i\rho}$ are, obtained from a (hypothetical) equilibrated stress field. Such a stress field can be obtained from the three-dimensional stress functions. To this end, we introduce the Beltrami stress function representation for stresses:

$$\sigma_x = \frac{\partial^2\chi_3}{\partial y^2} + \frac{\partial^2\chi_2}{\partial z^2} - \frac{\partial^2\psi_1}{\partial y\partial z}\ ; \quad \sigma_y = \frac{\partial^2\chi_1}{\partial z^2} + \frac{\partial^2\chi_3}{\partial x^2} - \frac{\partial^2\psi_2}{\partial z\partial x}\ ; \ \sigma_z = \frac{\partial^2\chi_2}{\partial x^2} + \frac{\partial^2\chi_1}{\partial y^2} - \frac{\partial^2\psi_3}{\partial x\partial y}\ ;$$

$$\sigma_{yz} = -\frac{\partial^2\chi_1}{\partial y\partial z} + \frac{1}{2}\frac{\partial}{\partial x}\left(-\frac{\partial\psi_1}{\partial x} + \frac{\partial\psi_2}{\partial y} + \frac{\partial\psi_3}{\partial z}\right)\ ; \quad \sigma_{zx} = -\frac{\partial^2\chi_2}{\partial z\partial x} + \frac{1}{2}\frac{\partial}{\partial y}\left(\frac{\partial\psi_1}{\partial x} - \frac{\partial\psi_2}{\partial y} + \frac{\partial\psi_3}{\partial z}\right)\ ;$$

$$\sigma_{xy} = -\frac{\partial^2\chi_3}{\partial x\partial y} + \frac{1}{2}\frac{\partial}{\partial z}\left(\frac{\partial\psi_1}{\partial x} + \frac{\partial\psi_2}{\partial y} - \frac{\partial\psi_3}{\partial z}\right)\ . \tag{21}$$

where (χ_1,χ_2 and χ_3) are Maxwell's stress functions, and (ψ_1,ψ_2 and ψ_3) are Morera's stress functions. For simplicity, we present here only the stress function assumptions based on Maxwell's representation. Since the tractions generated from the above stress field have to be evaluated on the faces of the singular element, it is convenient to assume the stress function in terms of curvilinear coordinates ξ, η and ζ. For reasons discussed in Section 3.1, the three stress-functions (χ_1,χ_2,χ_3) were assumed with a total of 54 undetermined parameters in them. Out of these, 51 basis functions were of regular polynomial nature and the other 3 had a $1/\sqrt{r}$ variation in them. Each of the 54 basis functions in the three stress-function assumptions should be such that it does not produce a stress tensor that is linearly dependent on the stress tensor produced by the other 53 basis functions. Another necessary condition in the proper choice of these stress function is shown in [Ref. 13] to be that the matrix $[P_1]$ represented in the scalar

$$[\beta]^T[P_1]\{\alpha\} = \int_{\partial\Omega_m} [\beta]^T[U_R]^T[R_S]\{\alpha\}\ ds \tag{22}$$

(where α are parameters in boundary tractions $\{T_{i\rho}\} = [R_S]\{\alpha\}$) be non-singular. Thus, considerable care had to be exercised in properly chosing the stress function below such that they produce the needed stress modes, and these are given below:

$$\chi_1 = \alpha_1\eta^2 + \alpha_2\eta\zeta + \alpha_3\xi\eta^2 + \alpha_4\xi\zeta^2 + \alpha_5\eta\zeta^2 + \alpha_6\eta^2\zeta + \alpha_7\xi\eta\zeta + \alpha_8\eta^3\zeta^2 + \alpha_9\xi\eta^2\zeta + \alpha_{10}\xi\eta\zeta^2$$
$$+ \alpha_{11}\eta^3\zeta + \alpha_{12}\eta\zeta^3 + \alpha_{13}\xi\zeta^3 + \alpha_{14}\xi^2\eta^2 + \alpha_{15}\eta^2\zeta^2 + \alpha_{16}\xi^2\zeta^2 + \alpha_{17}\eta^4\zeta\ .$$

$$\chi_2 = \alpha_{18}\zeta^2 + \alpha_{19}\xi\zeta + \alpha_{20}\eta\zeta^2 + \alpha_{21}\xi^2\eta + \alpha_{22}\xi^2\zeta + \alpha_{23}\xi\zeta^2 + \alpha_{24}\xi\eta\zeta + \alpha_{25}\xi^2\zeta^3$$
$$+ \alpha_{26}\xi\eta\zeta^2 + \alpha_{27}\xi^2\eta\zeta + \alpha_{28}\xi\zeta^3 + \alpha_{29}\xi^3\zeta + \alpha_{30}\xi^3\eta + \alpha_{31}\eta^2\zeta^2 + \alpha_{32}\xi^2\zeta^2$$

$$+ \alpha_{33}\xi^2\eta^2 + \alpha_{34}\xi\zeta^4$$

$$x_3 = \alpha_{35}\xi^2 + \alpha_{36}\xi\eta + \alpha_{37}\xi^2\zeta + \alpha_{38}\eta^2\zeta + \alpha_{39}\xi\eta^2 + \alpha_{40}\xi^2\eta + \alpha_{41}\xi\eta\zeta + \alpha_{42}\xi^3\eta^2$$

$$+ \alpha_{43}\xi^2\eta\zeta + \alpha_{44}\xi\eta^2\zeta + \alpha_{45}\xi^3\eta + \alpha_{46}\xi\eta^3 + \alpha_{47}\eta^3\zeta + \alpha_{48}\xi^2\zeta^2 + \alpha_{49}\xi^2\eta^2$$

$$+ \alpha_{50}\eta^2\zeta^2 + \alpha_{51}\xi^4\eta \; . \tag{23}$$

Setting for convenience, ($\chi_1 = x$, $\chi_2 = y$, $\chi_3 = z$; and $\xi_1 = \xi$, $\xi_2 = \eta$, and $\xi_3 = \zeta$), one can write

$$\frac{\partial^2 \chi_k}{\partial\xi_i\partial\xi_j} = \frac{\partial \chi_k}{\partial x_m}\frac{\partial^2 x_m}{\partial\xi_i\partial\xi_j} + \frac{\partial^2 \chi_k}{\partial x_m\partial x_n}\frac{\partial x_m}{\partial\xi_i}\frac{\partial x_n}{\partial\xi_j} \tag{24}$$

and calculate the stresses σ_{ij} according to Eq. (21), from which the boundary tractions are derived as $T_{i\rho} = \sigma_{ij}\,\eta_j$. The remaining three traction modes in $T_{i\rho}$ are assumed from the singular stress field given in Eq. (3) wherein (K_1, K_2, K_3) are replaced by α_{52}, α_{53} and α_{54} respectively.

4. Some Details of the Numerical Procedure:

By expressing the differential volume dv as $dv = \det J \; d\xi \; d\eta \; d\zeta$, the numerical integration of the volume integral for the strain energy, for each element, due to the assumed "regular" displacements (with β's) was carried out by using a 27 point non-product quadrature rule suggested by Irons [17]. As mentioned earlier, the strain energy due to the assumed singular functions can be evaluated, equivalently, by surface integrals that are either free from singularities, or contain a $1/\sqrt{r}$ variation over the surface. We express the differential area (dA) on a face such as BCGF (with $\xi = +1$) in Fig. 2b, as $dA = (\partial\vec{R}/\partial\eta) \times (\partial\vec{R}/\partial\zeta)\, d\eta\, d\zeta$, where $\vec{R} = (\vec{i}x + \vec{j}y + \vec{k}z)$. By using this, the above mentioned area integrals, and others occuring in the functional of Eq. (5), are evaluated by using a 37 point non-product quadrature rule due to Rabinowitz and Richter [18]. We also mention that as a variation of the assumptions described in Section 3, the stress intensity factors K_I, K_{II} and K_{III} themselves were allowed to be quadratic functions of the crack-front coordinate η (Fig. 2b). In this case, the asymptotic singular solution will not be equilibrated a priori, and thus the strain energy corresponding to the singular strains had to be evaluated by volume integrals with 1/r singularities. This integration had to be done by product-Gaussian formulae using as many as 340 points. Finally we comment on the solution technique for the final algebraic equations represented by:

$$[\,\mathbb{K}_S] \left\{\begin{Bmatrix} q^* \\ \underset{\sim}{K} \end{Bmatrix}\right\} \equiv \begin{bmatrix} \mathbb{K}_1 & \mathbb{K}_2^T \\ \mathbb{K}_2 & \mathbb{K}_3 \end{bmatrix} \begin{Bmatrix} q^* \\ \underset{\sim}{K} \end{Bmatrix} = \begin{Bmatrix} Q_1 \\ Q_2 \end{Bmatrix} \tag{25}$$

In the above, $\mathbb{K}_1$ is the usual banded symmetric form, where as $\mathbb{K}_2$ and $\mathbb{K}_3$ destroy the banded property of the entire matrix on the L.H.S. of Eq. (25). To solve Eq. (25), one can use the Fadeev and Faddeeva [19] technique to achieve a L, U decomposition of $[\,\mathbb{K}_S]$ as:

$$[\,\mathbb{K}_S] = [L][U] = \begin{bmatrix} L_{11} & 00 \\ L_{21} & L_{22} \end{bmatrix} \begin{bmatrix} U_{11} & U_{12} \\ 0 & U_{21} \end{bmatrix} \tag{26}$$

Thus, $\mathbb{K}_1 = L_{11}U_{11}$; $\mathbb{K}_2^T = L_{11}U_{12}$; $\mathbb{K}_3 = L_{21}U_{12} + L_{22}\,U_{22}$. Thus, L_{11} and U_{11} are the decompositions for the usual stiffness matrix K_1 and can be obtained separately. The unkowns $\underset{\sim}{q}^*$ and intensity factors $\underset{\sim}{K}$ are then solved in the usual way, except double precision may be needed in decomposing K_2 and K_3.

5. Element Evaluation and Results:

Because of the considerable soft-ware problems involved in computing realistic engineering fracture mechanics problems using the present three-dimensional finite element development, simple test cases were first devised to check the accuracy of the present method. First, a single "singular-element", for instance the element with $0 < \theta < \pi/2$ in Fig. 3, was considered. The relevant equations for this single element under the present method, are

$$\underset{(63\times 63)}{\begin{bmatrix} K_1 & K_2 \\ K_2^T & K_3 \end{bmatrix}} \underset{(63\times 1)}{\begin{Bmatrix} \underset{\sim}{q} \\ \underset{\sim}{K} \end{Bmatrix}} = \underset{(63\times 1)}{\begin{Bmatrix} \underset{\sim}{Q} \\ 0 \end{Bmatrix}} \qquad \begin{matrix} (27a) \\ (27b) \end{matrix}$$

where $\underset{\sim}{q}$ are the 60 nodal displacements, $\underset{\sim}{K}$ the 3 elastic intensity factors and $\underset{\sim}{Q}$ the equivalent nodal loads. For this singular element, element nodal displacements were first computed from the known analytical asymptotic solution, viz., Eq. (2) corresponding to a hypothetical mixed mode loading which generates the intensity factors to be $K_1 = K_2 = K_3 = 1.0$. Using these $\underset{\sim}{q}$ as input conditions, from the numerically generated matrices K_2^T and K_3, the results for K_1, K_2 and K_3 are computed from Eq. (27b). The computed results were,

$$K_1 = 0.97424 \; ; \; K_2 = 1.00791 \; ; \; K_3 = 1.00019 \tag{28}$$

which compare favorably with input values of $K_1 = K_2 = K_3 = 1.0$. Corresponding to asymptotic stress field of Eq. (3), with input values $K_1 = K_2 = K_3 = 1$, the equivalent nodal loads $\underset{\sim}{Q}$ were also computed. Using the input values of $\underset{\sim}{q}$, and the computed K's as in Eq. (28), the left hand side of Eq.(27a) was computed and compared with the right hand side input values of $\underset{\sim}{Q}$. This comparison was found to be good to a third digit accuracy. The above procedure was repeated for three other "singular" elements ($\pi/2 < \theta\ \pi$, $\pi < \theta < 3\pi/2$, $3\pi/2 < \theta < 2\pi$), and the above mentioned checks were equally valid in all the three cases. As a second check, a four-element assembly as shown in Fig. 3 was considered. The displacements at the nodes on the boundary of this four-element assembly were computed from the known analytical asymptotic solution, Eq. (2), with hypothetical input values $K_1 = K_2 = K_3 = 1$. Using the equation similar to Eq. (27b) above for this four-element assembly, the numerical solution for K's were computed, which are:

$$K_1 = 0.98361 \; ; \; K_2 = 0.98764 \; ; \; K_3 = 0.99945$$

The "internal" nodal forces were then computed from the left-hand-side of an equation similar to Eq. (27a) and were compared with the "external" nodal forces $\underset{\sim}{Q}$ computed from the asymptotic stress field with input values $K_1 = K_2 = K_3 = 1$. This comparison was also good to a third digit accuracy.

The computer program was then extended to solve a through-the-thickness crack in a tension plate using 24 elements, and an embedded elliptical crack in a tension specimen, subjected to modes I and II loads. These results are not presented here for want of space.

Conclusions: A detailed discussion on a three-dimensional finite element method, using embedded singularities, and based on the displacement-hybrid model is presented and some simple evaluations of the procedure are presented. The present "singular" element may be incorporated into existing sophisticated three-dimensional finite-element software by researchers having access to such software.

Acknowledgement: This work was supported by the U.S. AFOSR Grant 74-2667. The encouragement of Dr. W. J. Walker is gratefully appreciated.

References:

[1] Sneddon, I. N., Proceedings of the Royal Society, Series A, Vol. 187, 1946, pp. 229-260.

[2] Sadowsky, M. A. and Sternberg, E., Journal of Applied Mechanics, Trans. ASME, Series E, Vol. 16, 1949, pp. 149-157.

[3] Green, A. E. and Sneddon, I. N., Proceedings of the Cambridge Philosophical Society, Vol. 46, 1950, pp. 159-163.

[4] Shah, R. C. and Kobayashi, A. S., International Journal of Engineering Fracture, Vol. 3, No. 1, 1971, pp. 71-96.

[5] Shah, R. C. and Kobayashi, A. S., In, Stress Analysis and Growth of Cracks, Part I, ASTM STP 513, 1972, pp. 3-21.

[6] Smith, F. W., et al., Journal of Applied Mechanics, Vol. 34, Trans. ASME, Series E, Dec. 1967, pp. 953-959.

[7] Smith, F. W. and Alavi, M. J., Proceedings of the First Internation Conference on Pressure Vessel Technology, Delft, Holland, 1969.

[8] Kassir, M. K. and Sih, G. C., Journal of Applied Mechanics, Vol. 33, Trans. ASME, Series E., 1966, pp. 601-611.

[9] Tong, P and Pian, T. H. H., International Journal of Solids and Structures, Dec. 1973, pp. 313-321.

[10] Byskov, E., International Journal of Fracture Mechanics, Vol. 6, No. 2, June 1970, pp. 159-167.

[11] Pian, T. H. H., Tong, P. and Luk, C. H., Proceedings of the Third Conference on Matrix Methods in Structural Mechanics, Wright-Patterson, AFB, 1972.

[12] Tong, P., Pian, T. H. H. and Lasry, S., International Journal of Numerical Methods in Engineering, Vol. 7, No. 3, 1973.

[13] Atluri, S., Kobayashi, A. S., and Nakagaki, M. "An Assumed Displacement Hybrid Finite Element Model for Linear Fracture Mechanics," International Journal of Fracture Mechanics, in print.

[14] Atluri, S., Kobayashi, A. S. and Nakagaki, M., "Application of an Assumed Displacement Hybrid Finite Element Model to Two-Dimensional Problems of Fracture Mechanics," AIAA Journal, in print.

[15] Sih, G. C., Mechanics of Analysis and Solution of Crack Problems, Vol. 1, (G. C. Sih, Editor) Noordhoff International Publishing, Leydon, 1973, pp. XXI-XLV.

[16] Tong, P., International Journal of Numerical Methods in Engineering, 2, 1970, pp.73-83.

[17] Irons, B. M., International Journal for Numerical Methods in Engineering, 3, No. 2, 1971, pp. 293-294.

[18] Stroud, A. H., Approximate Calculation of Multiple Integrals, McGraw-Hill, New York, 1971.

[19] Faddeev, D. K. and Faddeeva, U. N., Computational Methods of Linear Algebra, Dover, New York, 1963.

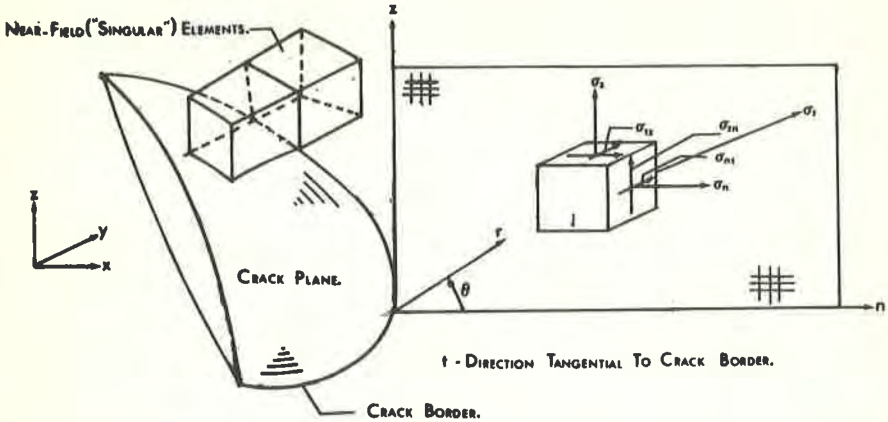

FIG.1. NOMENCLATURE NEAR CRACK FRONT.

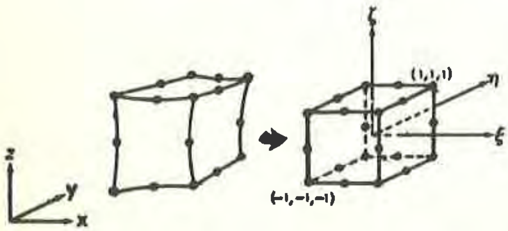

FIG.2a. THREE-DIMENSIONAL MAPPING.

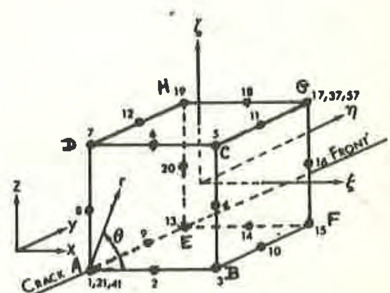

DISPLACEMENTS IN CARTESIAN DIRECTIONS.

FIG.2b. NODAL DISPLACEMENTS (CARTESIAN).

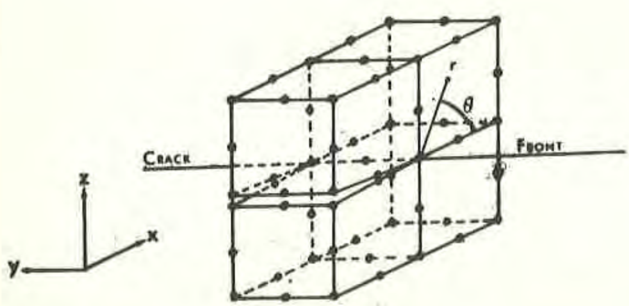

FIG.3. FOUR-ELEMENT ASSEMBLY SUBJECTED TO COMBINED MODE (k_I, k_{II}, k_{III}) LOADINGS.